Provided for non-commercial research and education use.
Not for reproduction, distribution or commercial use.

Volumes 403 Issue 1 1 January 2008 ISSN 0921-4526

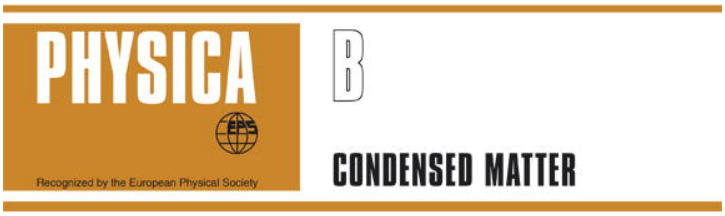

Editors:

F.R. DE BOER
P.E. BROMMER
L. DEGIORGI
R. JOCHEMSEN
H. WADA

Available online at
ScienceDirect
www.sciencedirect.com

http://www.elsevier.com/locate/physb

This article was published in an Elsevier journal. The attached copy is furnished to the author for non-commercial research and education use, including for instruction at the author's institution, sharing with colleagues and providing to institution administration.

Other uses, including reproduction and distribution, or selling or licensing copies, or posting to personal, institutional or third party websites are prohibited.

In most cases authors are permitted to post their version of the article (e.g. in Word or Tex form) to their personal website or institutional repository. Authors requiring further information regarding Elsevier's archiving and manuscript policies are encouraged to visit:

http://www.elsevier.com/copyright

Author's personal copy

Available online at www.sciencedirect.com
ScienceDirect
Physica B 403 (2008) 207–218
PHYSICA B
www.elsevier.com/locate/physb

Temperature dependence of the EPR lines in weakly doped $LiNbO_3$:Yb—possible evidence of Yb^{3+} ion pairs formation

Tomasz Bodziony*, Slawomir M. Kaczmarek, Czeslaw Rudowicz

Institute of Physics, Szczecin University of Technology, Al. Piastów 17, 70310 Szczecin, Poland

Received 7 June 2007; received in revised form 13 August 2007; accepted 27 August 2007

Abstract

The electron paramagnetic resonance (EPR) studies of $LiNbO_3$ single crystal doped with 1 wt% of Yb^{3+} are reported. To put the EPR results in perspective, a brief discussion of optical absorption spectroscopy investigations of $LiNbO_3$:Yb^{3+} is provided. The temperature behavior of the EPR lines intensity and linewidth for $LiNbO_3$:Yb^{3+} reveals antiferromagnetic coupling between Yb^{3+} ions. The deconvolution of the EPR lines indicates that EPR signals arise from both the isolated Yb^{3+} ions as well as the Yb^{3+}–Yb^{3+} ion pairs; the latter signals dominate. Based on this indication, EPR spectra are interpreted using a spin Hamiltonian for the Yb^{3+} dissimilar ion pairs. The negative sign of the isotropic parameter J confirms the existence of the antiferromagnetic interactions within Yb^{3+}–Yb^{3+} pairs. The value of J obtained based on the proposed pair model, assuming the dipole–dipole interactions, is used to identify the positions of the Yb^{3+}–Yb^{3+} pairs in the unit cell. Our results suggest the $^{even}Yb^{3+}$–$^{even}Yb^{3+}$ pairs are located at the neighboring Li^+ and Nb^{5+} positions, whereas the pair axis is not parallel to the optical c-axis. Some alternative explanations of the observed EPR spectra are also considered.
© 2007 Elsevier B.V. All rights reserved.

PACS: 76.30.−v; 75.30.Hx; 75.10.Dg; 76.30.Kg; 78.30.−j; 78.55.−m

Keywords: Electron paramagnetic resonance (EPR); Exchange and superexchange; Rare-earth ions; Ytterbium ions; Spin-Hamiltonian parameters; Lithium niobate crystals ($LiNbO_3$); Pairs of ions

1. Introduction

Lithium niobate $LiNbO_3$ (LN) is one of the best studied ferroelectric, electro-optic materials, see e.g. the reviews [1,2]. Structural properties and phase transitions as well as luminescence, Raman and electron paramagnetic resonance (EPR/ESR) spectra of LN have been reviewed in Refs. [3,4]. Interest in LN is driven by its unusual nonlinear electric, magnetic, and acousto-optic properties, which have been utilized for various technological applications. Doping with trivalent transition ions, especially rare-earth (RE) elements, has pronounced effect on some properties of $LiNbO_3$, e.g. structure, electro-optical coefficients, and light absorption. Fine-tuning these properties by doping opens wide possibilities of improving the important technological applications focused on electro-optic devices used for, e.g. information storage, holography, planar waveguide lasers, and amplifiers. In general, the optical properties of doped crystals are largely determined by the local site symmetry of the optically active ions.

The space group of $LiNbO_3$ crystal is trigonal: R3c (C_{3v}^6). The unit cell of LN is rhombohedral with the lattice constants at 296 K, $a=0.514829$ nm and $c=1.38631$ nm [4,5]. In the LN structure the oxygen atoms are arranged in planar sheets forming a network of trigonally distorted octahedra, which are adjoined by walls forming chains along the crystallographic c-axis being the optical axis. The sequence of octahedra repeats as {Nb, vacancy, Li} [4–6]. The RE impurity ions in LN may occupy one of the four sites, namely, three octahedral sites: Li^+, Nb^{5+} or cation vacancy, and the tetrahedral interstitial site. It has been shown that the trivalent RE ions occupy mostly Li^+ sites

*Corresponding author. Tel.: +48 91 449 4032; fax: +48 91 434 2113.
E-mail address: tbodziony@ps.pl (T. Bodziony).

0921-4526/$ - see front matter © 2007 Elsevier B.V. All rights reserved.
doi:10.1016/j.physb.2007.08.224

Author's personal copy

and are located off-center from the regular Li^{+} positions towards the structural vacancy octahedral sites along *c*-axis [7,8]. Thus, the RE^{3+} ions can be distributed in the crystallographically inequivalent centers in this host, giving rise to different sets of optical transitions [8]. Several experimental and theoretical studies have indicated that RE ions in LN occupy also the Nb^{5+} sites [9–19]. $LiNbO_3$ is usually grown from congruent melt compositions with Li^{+} to Nb^{5+} concentration ratio of the order of 0.945 giving rise to the Li-deficient crystals that need intrinsic defects to satisfy the overall charge compensation. It is generally accepted [10,11] that the Li-deficiency in LN single crystals is compensated by a certain amount of Nb^{5+} ions located at the Li^{+} sites, the so-called anti-sites. For a given RE^{3+} dopant ion, various crystallographically inequivalent centers may occur, whereas the relative concentration of such centers depends on the stoichiometry (i.e. the Li/Nb concentration ratio). This result indicates that the nature of the RE^{3+} centers in LN is directly related to the defects associated with the non-stoichiometric conditions.

The EPR spectroscopy of trivalent ytterbium (Yb^{3+}) in LN was investigated by Burns et al. [10] and Bonardi et al. [11], whereas Dong et al. [17] studied theoretically the spin-Hamiltonian (SH) parameters for Yb^{3+} ions in LN:Yb^{3+}, Mg^{2+} single crystals. The studies [10,11,17] indicate that the site symmetry of Yb^{3+} centers is C_3 and Yb^{3+} ions occupy mainly the Li^{+} sites. In $LiNbO_3$:Mg, Yb, the Yb^{3+} ions may also occupy Nb^{5+} sites due to MgO co-dopant [17]. Choh et al. [18] arrived at similar conclusion for Er^{3+} in Er and Mg co-doped LN single crystals. The structural analysis by Malovichko et al. [20,21] reveals that the RE ions enter octahedral sites in $LiNbO_3$, which may exhibit either the C_3 or the C_1 site symmetry. Montoya et al. [22] study of cooperative luminescence in $LiNbO_3$:Yb^{3+} provided a firm evidence of the Yb^{3+} pairs in this matrix. Subsequently, Montoya et al. [23] proposed three models for Yb^{3+} ions distribution in $LiNbO_3$:MgO and related each model to the observed features of cooperative luminescence. LN crystals studied in Refs. [22,23] concerned low concentration of Yb doping. The experimental results [23] favor the Yb^{3+} distribution model in which a fraction of dopant ions (about 10.4 wt% of all Yb^{3+} ions) forms pairs with one Yb^{3+} ion placed at the Li^{+} site and another one at the Nb^{5+} site, while the rest of the Yb^{3+} ions are randomly distributed at the Li^{+} sites [23].

Our previous studies [24–26] focused on spectroscopic investigations of LN single crystal doped with Yb ions and/or co-doped with Pr ions. No RE impurity centers with C_3 site symmetry in LN host were clearly observed by us. We have found that Yb^{3+} ions predominantly occupy sites with lower C_1 symmetry in both LN: Yb, Pr and LN:Yb crystals [25,26]. In this paper EPR study of Yb^{3+} ions in LN crystal doped with Yb (1 wt%) are reported. In Section 2 the sample details and general experimental conditions are outlined. Optical spectroscopy studies are briefly discussed in Section 3 to put in perspective the EPR results. Analysis of the EPR spectra and their temperature dependence in terms of a model of Yb ion pairs is carried out in Section 4. This enables identification of the positions of the Yb^{3+}–Yb^{3+} pairs in the unit cell. Since changes of the EPR line profiles may also be related to several inequivalent Yb^{3+} centers, the counterarguments against this alternative explanation are discussed. In Section 5 we provide summary and conclusions.

2. Sample and experimental details

$LiNbO_3$ single crystal doped with 1 wt% of Yb^{3+} was grown along *c*-axis from the congruent melt by the Czochralski method in the Institute of Electronic Materials Technology (IEMT, Warsow, Poland). The Yb concentration was 1% molar fraction in the melt. The following starting materials were used: Nb_2O_5 (4 N purity) from Johnson-Matthey; Li_2CO_3 (4 N purity) from IEMT. After mixing of adequate amounts of reagents the mixture was calcined at 1373 K for 6 h. The Yb_2O_3 was added to the charge of congruent melt with the Li/Nb ratio equal 0.94, prior to synthesis at elevated temperatures. The growth conditions were as follows—growth rate: 1–2 mm/h, rotation rate: 5–20 rpm, axial temperature gradient over melt: 10–30°/cm, atmosphere: air. The temperature gradient was regulated through shifting the crucible in the afterheater as well as the crucible-afterheater system w.r.t. the induction coil. A more detailed description of the applied growth process is presented elsewhere [27].

The LN:Yb samples used for EPR studies were cut out from the bulk sample oriented at room temperature using the X-ray diffraction method (XRD) and polished. The samples had the form of parallel plates of dimensions $3.1 \times 2.7 \times 1.5$ mm with the surfaces perpendicular to *c*-axis determined from XRD. The laboratory axis system (*X*, *Y*, *Z*) was chosen as follows: *Z*-axis was taken along the crystallographic (i.e. optical) *c*-axis, *X*-axis along the one of the crystallographic *a*-axis and *Y*-axis as perpendicular to both *Z*- and *X*-axes. Because EPR signals of RE ions can be observed mainly at liquid-helium temperature, EPR spectra were recorded using Bruker E 500 X-band spectrometer ($\nu \sim 9.4$ GHz) with 100 kHz field modulation equipped with Oxford flow cryostat for measurements at temperatures from liquid nitrogen one down to 4 K. The samples were mounted on a goniometer to measure the angular dependence of the spectra; however, the pre-oriented samples could not be rotated in two planes inside the cryostat during EPR measurements.

3. Optical spectra

The optical spectra of LN:Yb^{3+} single crystal, presented in Fig. 1, consist of intense sharp absorption bands, due to the $^2F_{7/2} \rightarrow {}^2F_{5/2}$ electronic transitions, and weak bands, due to the vibronic transitions or low symmetry effects superimposed onto wide continuous absorption of the host lattice. Pair absorption of the Yb^{3+} ions is not observed

Author's personal copy

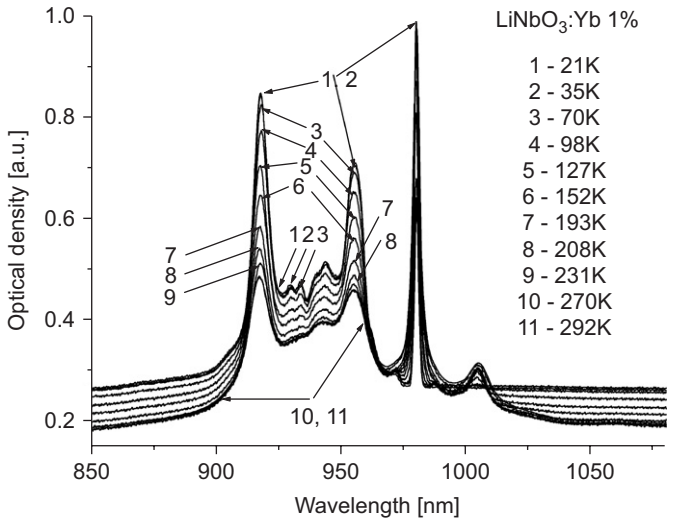

Fig. 1. Optical density of $LiNbO_3$:Yb (1 wt%) single crystal for several temperatures from 21 to 292 K.

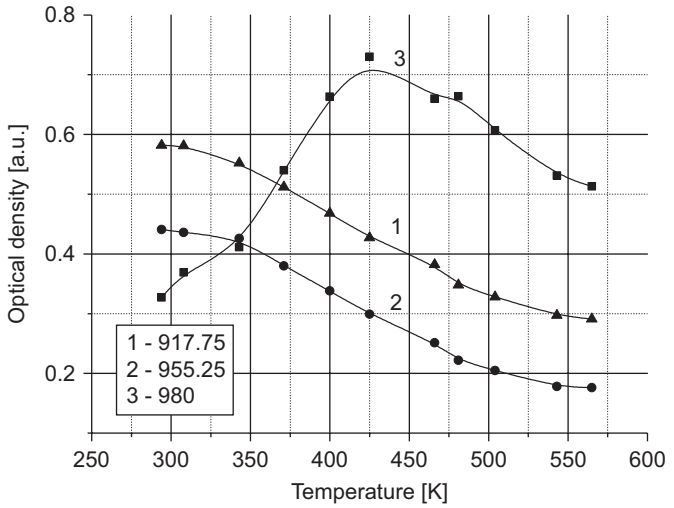

Fig. 2. Temperature dependence of the three basic absorption lines due to Yb^{3+} in $LiNbO_3$:Yb (1 wt%).

due to too low concentration of impurity ions. Nevertheless, the main 980 nm line has a maximum at about 423 K (see Fig. 2). The shape of the temperature dependence (a maximum) of this line suggests the presence of localized phonons near Yb^{3+} ion, which may be due to, e.g. another Yb^{3+} ion in the vicinity [24,28]. Moreover, the 2866 nm centered OH^- band, reveals shifting towards shorter wavelengths as compare to pure LN crystal (2873 nm centered for pure LN) and complex asymmetric shape, confirming the presence of some complex defect structure near Yb^{3+} ions. The observed hot bands (1004 and 1060 nm in Fig. 1) yield the excited levels arising from the $^2F_{7/2}$ and $^2F_{5/2}$ multiplets of Yb^{3+} ion in the C_3 crystal field (CF) [24,28].

Let us consider the possible low symmetry effects in our optical spectra. RE^{3+} ions in LN usually enter the Li^+ sites with C_3 symmetry [29]. Group theory predicts that the free ion multiplets $^2F_{7/2}$ and $^2F_{5/2}$ split, respectively, into four (E_1) and three (E_2) doubly degenerate CF levels in C_3 symmetry [30,31]. Spectroscopic studies of Yb^{3+} ions in various low symmetry crystals have been carried out by, e.g. Haumesser et al. [32] and Campos et al. [33]. As pointed out by Haumesser et al. [32], who carried out analysis of the CF strength (so without determination of the CF parameters) for Yb^{3+} ions in various Yb-doped laser materials, it is impossible to fit 27 CF parameters required for Yb^{3+} (and other RE^{3+}) ions at triclinic (C_1, C_i) symmetry sites. The reason is that in the case of Yb^{3+} ions in crystals only six CF transitions are available. Moreover, in case when some isolated Yb^{3+} ions in LN:Yb would occur at sites with C_1 symmetry, no distinct features due to low symmetry, as e.g. splitting of some levels, could be observed in the CF energy levels [28,34].

No further splitting due to the CF of lower symmetry is allowed by group theory, since the C_3 symmetry CF levels are the Stark doublets described by appropriate linear combinations of the $|J\pm M_J>$ corresponding to a given value of the effective 'spin' $J=\frac{7}{2}$ or $\frac{5}{2}$. Such doublets can only be split by an external magnetic field. Hence, only some variations of the energy level values and also possibly their sequence may be expected due to the low symmetry CF components.

This makes it extremely difficult to distinguish any low symmetry effects in the optical spectra or to identify the CF transitions arising from Yb^{3+} ions located at various possible low symmetry sites. In view of this discussion, any additional line of distinct character observed in the optical spectra of $LiNbO_3$:Yb^{3+} may rather originate from other mechanisms than the low symmetry CF of isolated Yb^{3+} ions. This provides one more argument for the Yb^{3+}–Yb^{3+} pair mechanism discussed below.

4. EPR spectroscopy measurements

Representative EPR spectra of the LN:Yb^{3+} (1 wt.%) sample [24,25] taken at various angles in the plane (denoted XY) perpendicular to the crystal c-axis and the plane (ZX) containing the crystal c (Z)-axis are presented in Figs. 3 and 4, respectively. The spectra were also measured in a third plane (ZY) yielding similar angular dependencies as in Fig. 3. Depending on a given angle, two or three strong lines and additionally several weak lines are observed, which partially cannot be fully distinguished because of the low spectral resolution. The most important feature of the EPR spectra of LN:Yb^{3+} in Figs. 3 and 4 is their evident complexity. The angular dependence of the EPR lines indicates that the observed spectra result from superposition of lines of various nature, which may be amenable to alternative explanations. In general, superposition of various signals may arise from either magnetically inequivalent paramagnetic centers of the same type or crystallographically distinct centers of the same or different type [35]. Moreover, the angular dependence of the EPR lines exhibit behavior characteristic for very low symmetry sites

Author's personal copy

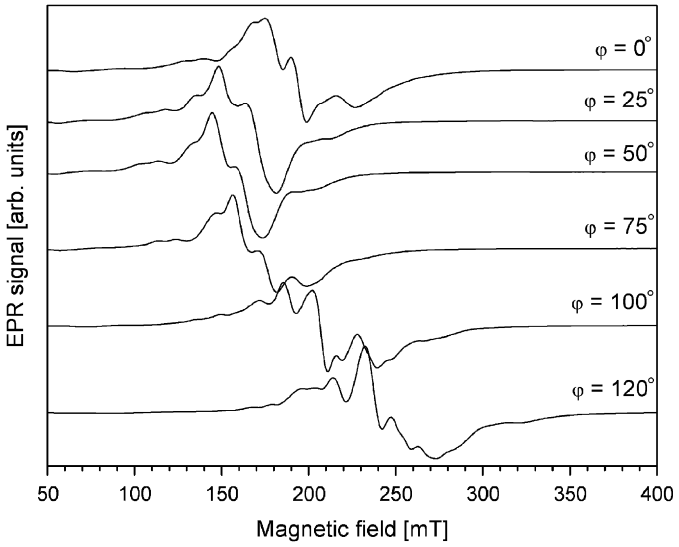

Fig. 3. Sample EPR spectra for the Yb^{3+}-doped LN crystal measured at 6–8 K temperature range in the plane (XY) perpendicular to the crystal c-axis ($\varphi = 0^\circ$ denotes X-axis).

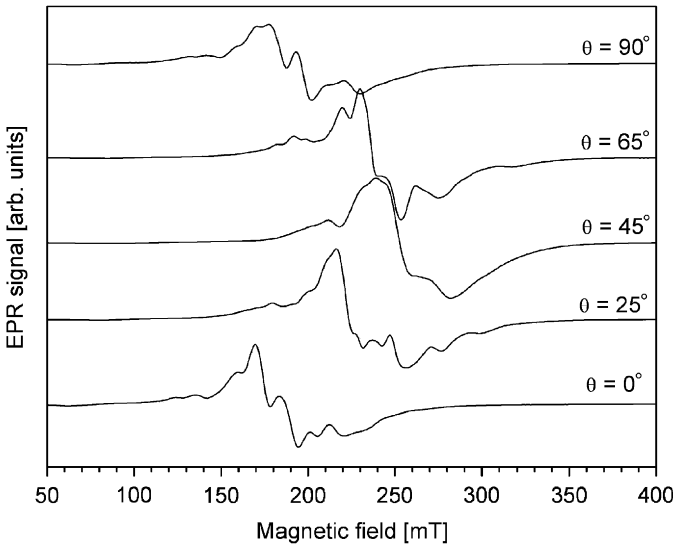

Fig. 4. Sample EPR spectra for the Yb^{3+}-doped LN crystal measured at 6–8 K temperature range in the plane (ZX) containing the crystal c-axis ($\theta = 0^\circ$ denotes Z-axis).

[36] as discussed in details below. It should be emphasized that we do not observe EPR spectra exhibiting axial symmetry observed in previous EPR studies [11]. It is worthwhile to consider the possible low symmetry effects in our EPR spectra similarly as discussed in Section 3 for the optical spectra. Detection of the possible low symmetry effects is much more feasible in EPR spectra, since it is a directional technique and enables better spectral resolution. On the basis of a thorough structural analysis and EPR studies of LN:Cr^{3+} Malovichko et al. [20,21] concluded that two symmetry options are possible for transition ion sites in LN, namely, C_3 (axial symmetry) and C_1. It should be noticed that only a hint of the low symmetry cases has been provided by Bonardi et al. [11], however, due to the low resolution neither these spectral lines have been analyzed nor the actual site symmetry identified. The authors [11] have also stated that the existence of Yb^{3+}–Yb^{3+} dimers cannot be rejected. Our earlier optical and EPR studies of LN:Yb, Pr and LN:Yb crystals have revealed isolated Yb^{3+} ions occupying C_1 symmetry sites [24–26].

Theoretically, the signals originating from isolated Yb^{3+} ions in LN host can be easily distinguished. At liquid helium temperature, depending on the relative concentration of various Yb isotopes, such spectra may show either a single central line originating from the fine structure transitions due to the ^{170}Yb even isotope (natural abundance: NA = 69.6%) with zero nuclear spin $I = 0$, and/or two hyperfine transitions distributed about a central line due to the ^{171}Yb odd isotope (NA = 19.3%) with $I = \frac{1}{2}$, and/or six hyperfine transitions distributed about a central line due to the ^{173}Yb odd isotope (NA = 16.1%) with $I = \frac{5}{2}$ [35]. This simple approach to identification of the EPR signals from isolated Yb ions was applied in our earlier work [24]. However, the observed EPR spectra of the LN:Yb^{3+} single crystal manifest also more sophisticated features (see Figs. 3 and 4). In Refs. [25,26], we have analyzed the optical and EPR spectra taking into account possibility of the existence of magnetically coupled pairs of Yb^{3+} ions in LN crystal.

The EPR spectra of similar ion pairs are characterized by a two-line pattern with each line having similar intensity, whereas those of dissimilar ion pairs by a four-line pattern, with the two middle lines much stronger in intensity then the two satellite lines. Some of the observed EPR spectra taken in all three perpendicular planes reveal a recognizable four-line pattern, which turns out to be characteristic for EPR spectra originating from the dissimilar RE ion pairs [37,38]. The line pattern is additionally more complicated, since in the case of LN impurity ions may occupy one of several (at least four) sites. Such situation additionally favors the option of the ion pairs with different g factors, i.e. dissimilar ion pairs [37,38]. In order to test the origin of this pattern further, we adopt the theoretical model of Yb ion pairs [25,26].

Based on the pair model developed below, which assumes interaction through space, the actual mechanism responsible for the magnetic interactions in the case of Yb–Yb ion pairs is ascribed to the magnetic dipole–dipole interaction [37,38]. It should be noticed that in the case of interaction through bonds the tensor would have a different nature, namely, the exchange (or superexchange) interaction between spins [38]. Taking into account the structure of the Li^+, Nb^{5+}, and O^{2-} ions in the vicinity of the Yb–Yb pair discussed in Section 4.2, it is evident that the oxygen ions do not intertwine between the Li^+ and Nb^{5+} ions in our model. Thus in the case of LN:Yb the Yb–Yb magnetic interaction would be through space, i.e. to the first approximation we may assume that the nature of this interaction is the magnetic dipole–dipole

Author's personal copy

interaction. The possibility of other interactions needs to be considered for the pair model involving interaction through bonds. Such option shall be dealt with in a future work.

The SH parameters were computed for the model of dissimilar RE ion pairs yielding the negative sign of the isotropic parameter $J = -0.028 \pm 0.001$ (cm^{-1}) [25]. This indicates the antiferromagnetic coupling between the Yb^{3+}–Yb^{3+} pair ions at temperature 8 K. Since the small value of root mean sum of squares of weighted differences between the observed and calculated resonance line positions (RMSD) [25] only indirectly confirms the model of the Yb^{3+}–Yb^{3+} ion pairs in LN crystal, an additional confirmation of the adopted model is needed. Hence, we have embarked on detailed analysis of the temperature dependence of the EPR spectra.

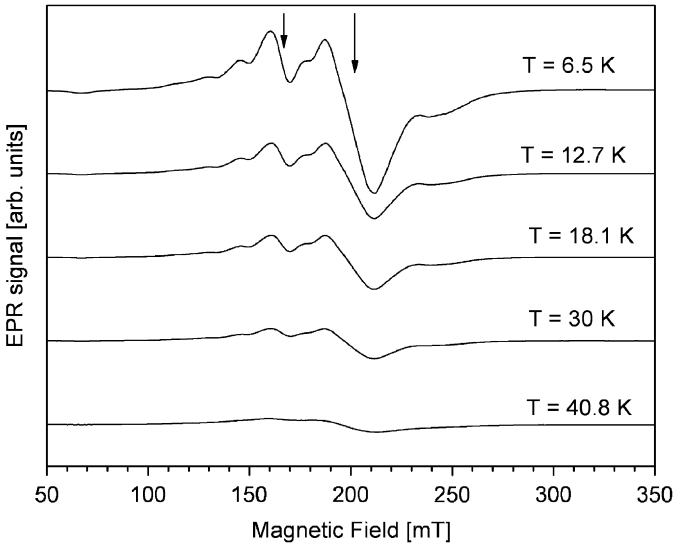

Fig. 5. Sample EPR spectra of $LiNbO_3$:Yb^{3+} crystal measured at various temperatures at a fixed angle ($\theta = 10^{\circ}$) in the plane ZY containing the crystal c-axis. Arrows indicate the lines 1 (left arrow) and 2 (right arrow) chosen for detailed analysis.

4.1. Analysis of the temperature dependence of EPR spectra

The EPR spectra taken in the temperature range from 6.5 K up to 41 K at a fixed angle ($\theta = 10^{\circ}$) in the ZY plane are presented in Fig. 5. One can recognize a strong line centered at about 165 (mT) (line 1 denoted by the left arrow) and a very strong line centered at about 200 (mT) (line 2 denoted by the right arrow). These are the best visible lines in the top EPR spectrum ($T = 6.5$ K). As discussed in Section 3, the optical measurements did not exclude the possibility of the existence of Yb ion pairs in LN:Yb single crystal. Question arises if the temperature dependence of EPR spectra confirms this finding. The best way to answer this question would be to perform a deconvolution of the spectra and study of the temperature dependence of the linewidth and the intensity of the individual lines observed in Fig. 5. The temperature dependence of the EPR linewidth for the two lines is presented in Fig. 6, whereas the EPR line intensity and the inverse intensity are shown in Fig. 7. The EPR line intensity was simply computed as the product of the square of the linewidth and the height of the line. Fig. 6 indicates that the EPR linewidth varies for the two lines in a similar way in the whole temperature range studied. When temperature decreases down to 20–24 K, the EPR linewidth of both lines decreases to a various extent for each line. In the temperature range from ~8 K up to ~20 K the EPR linewidth of both lines is subjected to small fluctuations.

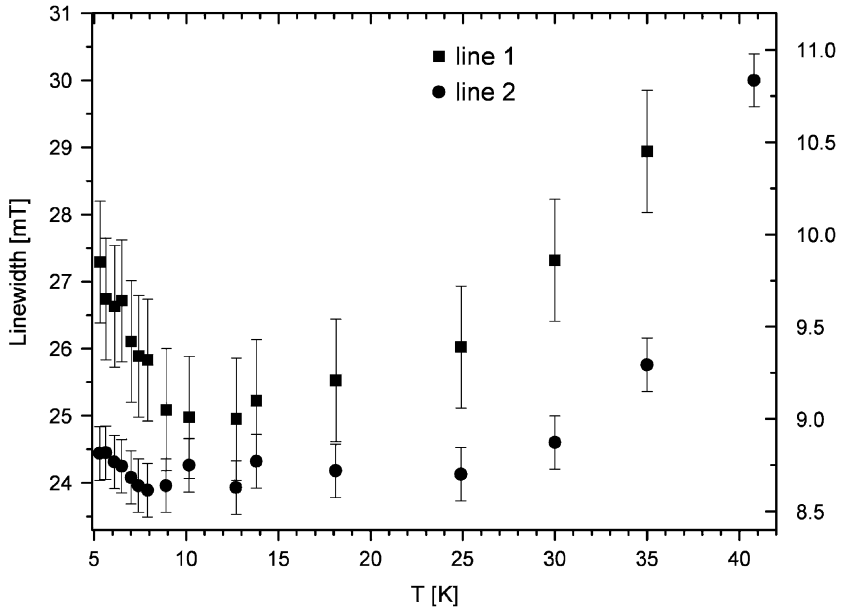

Fig. 6. The temperature dependence of the EPR linewidth for the two selected lines: line 1 (right axis, solid squares) and line 2 (left axis, solid dots) measured at a fixed angle ($\theta = 10^{\circ}$) in the plane ZY containing the crystal c-axis.

Author's personal copy

With further decrease of the temperature down to 5 K, the EPR linewidth of both lines start to increase to a various extent for each line. A weak minimum at about 7.9 K in the temperature dependence of the EPR linewidth of the line 2 is worth noting. The observed differences in the behavior of the EPR linewidth of both lines do not enable us to distinguish whether both lines arise from either (i) magnetically inequivalent paramagnetic centers of the same type, i.e. originate from the isolated Yb^{3+} ions, or (ii) the pairs of Yb^{3+} ions.

The increase of EPR linewidth with increasing temperature observed in the right part of Fig. 6 seems quite natural; however, the decrease of EPR linewidth with increasing temperature observed in the left part of Fig. 6 (below 10 K) comes as a surprise. This unusual behavior can be explained assuming that EPR lines 1 and 2 are superposition of signals arising from two different sources. First source, originating from isolated ^{even}Yb ions, dominates at the higher temperature region above 10 K, whereas the second one appears below this temperature and originates from ^{even}Yb–^{even}Yb ion pairs. Alternatively, the EPR signals recorded as lines 1 and 2 may be due to the ^{even}Yb–^{even}Yb ion pairs in the whole temperature range studied. The EPR line intensity as a function of a temperature (Fig. 7, upper panel) indicates that the line 2 is much stronger than the line 1, in spite of the fact that the two curves are shown in different scales. With decreasing temperature, the EPR line intensity of each line increases non-linearly. The sudden change of the EPR line intensity for the line 2 is observed between 7 and 7.4 K. Similar variation, but with considerably weaker changes, is observed in the temperature dependence of the EPR line intensity of the line 1. Fig. 7 (lower panel) indicates that the temperature dependence of the inverse intensity for each line is well described by a linear approximation in the temperature range from ~25 K down to ~7 K. This indicates the Curie–Weiss law is well obeyed for both lines in this temperature range. However, the linear approximation yields the model parameters that are essentially different for the two lines. The shape of the line 2 in Fig. 5 changes with temperature suggesting that this line may be a superposition of several lines arising from different paramagnetic centers.

To describe the asymmetrical shape of the line 2, we tentatively adopt three Lorentz lines, which is a reasonable minimum number of lines in a deconvolution. The first line reflects the small maximum visible near 175 (mT), the second and third line characterizes the shape of the main line. Fig. 8 shows the deconvolution of the EPR line 2 into the three constituent lines 2a, 2b, and 2c. One can see that the line being the sum of constituent lines (2a, 2b, 2c) reflects very well the shape of the line 2. This confirms the correctness of our approach. Fig. 9 presents the temperature dependence of the intensity for each of the three deconvoluted lines. The intensity of the EPR line 2 turns out to be dominated by the intensity of the line 2b. The intensity of the line 2c (Fig. 9, solid triangles) increases with

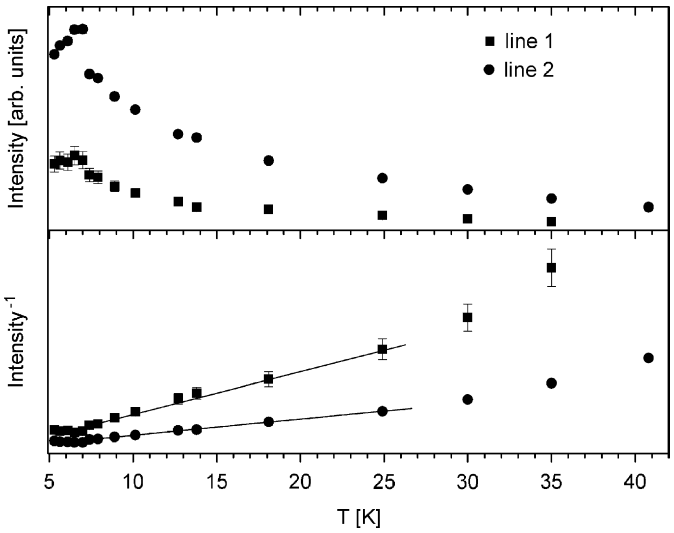

Fig. 7. Temperature dependence of the EPR line intensity (upper picture; different scale applies to each curve) and the inverse intensity (lower picture) measured at a fixed angle ($\theta = 10°$) in the plane ZY containing the crystal c-axis; line 1—solid squares, line 2—solid dots; experimental uncertainty indicated by the error bars is much less then the size of the data points.

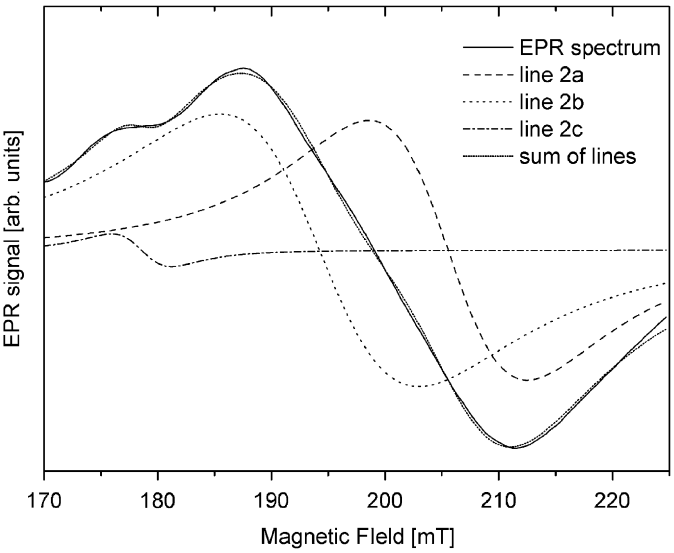

Fig. 8. Deconvolution of the EPR line 2 at $T = 12.7$ K into the three constituent lines 2a, 2b, and 2c.

decreasing temperature but very weakly, while that of the line 2a (Fig. 9, solid squares) increases with decreasing temperature. The intensity of the line 2b (Fig. 9, solid circles) increases with decreasing temperature, additionally showing a sudden increase at about 7.2 ± 0.2 K followed by a flattened decrease below this temperature. This disparate behavior of the three constituent lines indicates that the line 2b originates from other paramagnetic centers than the lines 2a and 2c.

The upper panel in Fig. 10 shows the dependence of the intensity of the lines 2a and 2c versus $1/T$, whereas the lower panel presents the inverse intensity of the line 2b

Author's personal copy

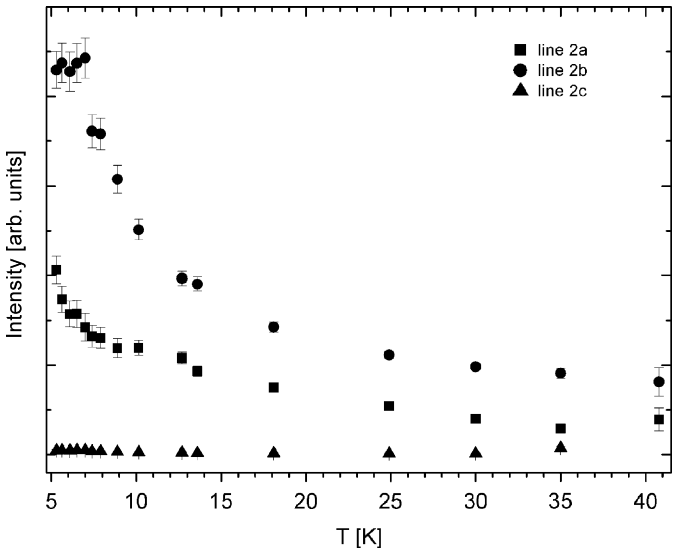

Fig. 9. The temperature dependence of the line intensity for the deconvoluted lines 2a, 2b, and 2c.

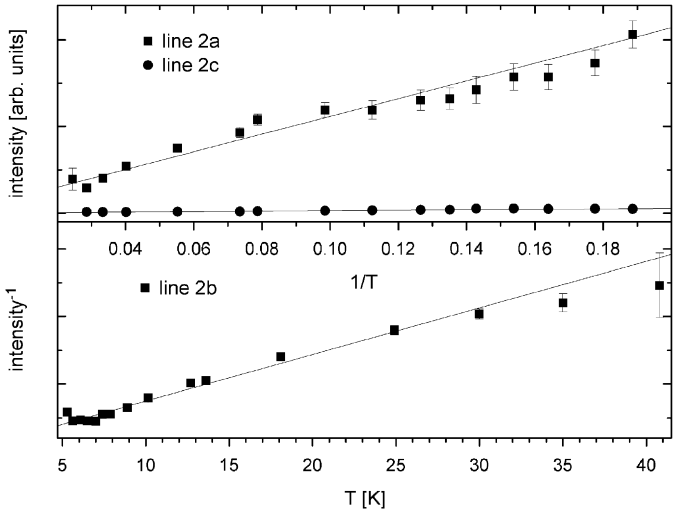

Fig. 10. The dependence of the intensity of the line 2a and 2c on $1/T$ (upper panel) and the inverse intensity of the line 2b on T (lower panel); solid lines are obtained by the linear fitting using the Curie law.

versus T. The best-fitted results (solid lines) obtained using the linear fit based on the Curie or the Curie–Weiss law are also presented in Fig. 12. It appears that intensity of the lines 2a and 2c obeys the Curie law, while the intensity of the line 2b may be well described by the Curie–Weiss law, apart from very low temperature range. Moreover, the behavior of the line 2b differs qualitatively from that of the lines 2a and 2c. These differences may be explained assuming that the lines 2a and 2c originate from the isolated Yb^{3+} ions, whereas the line 2b originates from the Yb^{3+}–Yb^{3+} ion pairs. The present deconvolution of line 2 confirms our earlier observation concerning the signals arising from isolated Yb^{3+} ions [24]. Due to similar characteristics of the lines 1 and 2 observed in Fig. 7, the line 1 appears to be also a superposition of the EPR signals

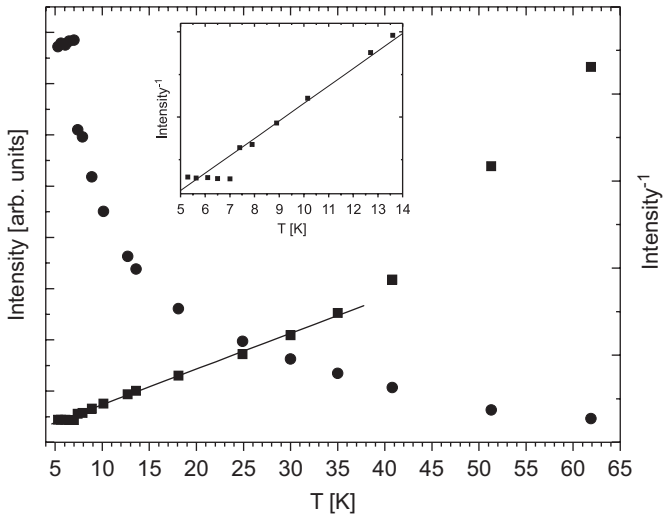

Fig. 11. The temperature dependence of the total EPR line intensity (left axis, solid dots) and its inverse (right axis, solid squares); experimental uncertainty is less then the size of the data points. The inset shows an enlarged section of the low temperature dependence of the inverse intensity revealing the unusual divergence from the Curie–Weiss law.

arising from qualitatively different paramagnetic centers, e.g. isolated Yb^{3+} ions and Yb^{3+}–Yb^{3+} ion pairs.

Finally, we consider the temperature dependence of the total EPR line intensity and its inverse presented in Fig. 11. The total intensity is calculated using double numerical integration of the EPR signal [35]. Generally, both the total intensity and its inverse vs T (Fig. 11) show behavior similar to that for the line 2, which predominates in the EPR spectra (see, Fig. 9). However, significant differences appear at temperatures above 30 K. Two distinct regions can be identified in the total inverse intensity diagram (solid squares): (i) low temperature one—between 5 and 40 K and (ii) higher temperature one—above 40 K up to 62 K, where the EPR lines disappear. In both regions the total inverse intensity vs T may be described well enough by the Curie–Weiss law. The EPR lines observed in the low temperature region arise predominantly from the Yb^{3+} centers. Above 40 K these EPR lines vanish and other lines of very low intensity start appearing. The origin of these lines is not clear at present. They may originate from some dopant paramagnetic ions, which enter the LN structure as impurities from the chemical ingredients during the crystal growth.

The observed behavior indicates that in the spectral region dominated by the EPR lines originating from the isolated Yb^{3+} ions the EPR line intensity satisfies the Curie–Weiss law. This enables us to determine the constant $\Theta = -0.6 \pm 0.3$ K. The negative Θ suggests that antiferromagnetic interactions may arise in the system of Yb^{3+} ions in LN. The temperature behavior of the total intensity and its inverse may possibly be explained by the presence of the antiferromagnetically coupled Yb^{3+} ion pairs in LN crystal, thus confirming the indications provided by our earlier EPR and optical measurements [25,26].

Author's personal copy

Analysis of the EPR measurements provides evidence of the existence of the Yb ion pairs in weakly doped LN:Yb^{3+} single crystal. However, a question arises: where are these pairs of ions located in the unit cell? Alternative explanation is considered in Section 4.3.

4.2. Position of Yb^{3+}–Yb^{3+} pairs in unit cell

We follow the SH used in Ref. [25] the effective SH characterizing the EPR spectra of the pairs of RE Kramers ions with the spin S^A and S^B can be written as a sum of the electronic Zeeman terms for each ion and the interaction term [35–38]:

$$H = \mu_B S^A \cdot g^A \cdot \vec{B} + \mu_B S^B \cdot g^B \cdot \vec{B} + S^A \cdot \widetilde{V} \cdot S^B, \quad (1)$$

where μ_B is the Bohr magneton and g^A (g^B) is the g-tensor for the ion A (B). Note that for Yb^{3+} ions the effective spin $S_{eff}=\frac{1}{2}$. The ion pairs can be either dissimilar, i.e. with a different g-tensor for each ion, or similar, i.e. with the same g-tensor for both ions [37,38].

According to the review [37] and assuming interaction through space (not through bonds), the actual mechanism responsible for the magnetic interactions in the case of Yb–Yb ion pairs is ascribed to the magnetic dipole–dipole interaction. Hence, we adopt the effective SH for the RE ion pairs in the general form [37,38]:

$$H = \mu_B S^A \cdot g^A \cdot \vec{B} + \mu_B S^B \cdot g^B \cdot \vec{B} + S^A \cdot \tilde{D}^{AB}_{dip} \cdot S^B, \quad (2)$$

where $\tilde{D}^{AB}_{dip}$,the magnetic dipole–dipole interaction is described by the well-known expression [35,36]:

$$\tilde{D}^{AB}_{dip} = \frac{\vec{\mu}^A \cdot \vec{\mu}^B}{R^3} - \frac{3(\vec{\mu}^A \cdot \vec{R}) \cdot (\vec{\mu}^B \cdot \vec{R})}{R^5}, \quad (3)$$

where $\vec{\mu}^A$ and $\vec{\mu}^B$ are the magnetic dipole moments of the ions A and B. Following the general approach [38], considerations reported in the magnetic spin–spin interactions between the two interacting spins A and B sufficiently removed one from the other, can be treated as interaction of two magnetic dipoles separated by R (the A–B distance). The last term in Eq. (3) can be divided into the isotropic part and the anisotropic one. For simplicity we use the symbol J for the isotropic parameter, which is calculated as the trace of the magnetic dipole–dipole tensor:

$$-2J = \frac{1}{3}\mathrm{Tr}\,\tilde{D}^{AB}_{dip}. \quad (4)$$

Based on the crystallographic data, two major options for the position of Yb^{3+}–Yb^{3+} pairs in the unit cell may be envisaged. First, we consider the possibility of the substitution of the two $^{even}Yb^{3+}$ ions forming the pair for (i) the Li^+ (or Nb^{5+}) and (ii) the structural vacancy. The distances between the Li^+ and Nb^{5+} ions located within the first and second coordination sphere in LN may be in the range from 0.305 to 0.515 nm [5,6,20,21]. The n.n. Li^+–Nb^{5+} distance equals 0.306 nm, while that of the Li^+–vacancy–Nb^{5+} is 0.388 nm. Substitution of the Yb^{3+} ions having the ionic radius of 0.100 nm at the vacancy position would lead to a large structural deformation (for the six-fold coordinated octahedral sites the ionic radius is equal to 0.090 nm for Li^+ and 0.078 nm for Nb^{5+}). Moreover, this substitution option should be accompanied by charge compensation, which may lead to creation of additional Li^+ and/or Nb^{5+} vacancies. Second, we consider the substitution of the Yb^{3+}–Yb^{3+} pair ions at the neighboring, i.e. the closest Li^+ and Nb^{5+} sites. A necessary condition for such option is the feasibility of substitution of Yb^{3+} both at the Li^+ sites as well as the Nb^{5+} sites. This option of substitution, which has an additional advantage as it requires no charge compensation, seems quite feasible.

Having determined the values of J (Eq. (4)) from the fitting procedure [25], we have attempted to identify the possible positions of the Yb_{Li} and Yb_{Nb} sites in LN lattice, involved in the Yb_{Li}–Yb_{Nb} pair formation. Based on the simple model of the magnetic dipole–dipole interactions we have analyzed all possible combinations inside the unit cell (Eq. (3)). We assume that those distinct pair locations, which yield large distortions, may be excluded. It should be mentioned that the positively charged Li^+ and Nb^{5+} ions, which are substituted by the Yb^{3+} dopant ions, are coordinated with the electronegative O^{2-} ions. For clarity, only some of the ions are shown in Fig. 12, namely, those forming octahedra around Li^+ and Nb^{5+} ions that counteract the possible large distortions in LN lattice. The two options for the pair formation outlined above may be further discussed in view of the analysis of ionic distances. The first option, namely, the substitution of the $^{even}Yb^{3+}$ pair ions, i.e. one Yb^{3+} ion at the Li^+ (or Nb^{5+}) sites and another at the structural vacancy site, may be excluded. Such option would lead to distortions much larger then 100% as compared with the undistorted host. As the second option, we have analyzed the Yb_{Li}–Yb_{Nb} pairs located at the neighboring Li^+ and Nb^{5+} sites. Our calculations have shown that this option yields the smallest distortion as compared with other locations for the pair ions. So, we may consider this option as the most feasible from the crystallographic and spectroscopic point of view. This pair type, i.e. the $^{even}Yb^{3+}$–$^{even}Yb^{3+}$ pair located at the n.n. Li^+–Nb^{5+} sites, is marked by a circle in Fig. 12. After formation of such pair at the positions of the indicated n.n. Li^+–Nb^{5+} ions, the distance between the pair ions changes from 0.307 to 0.409 nm yielding an increase of 34%. Li^+ and Nb^{5+} ions positions indicated in Fig. 12 are close to the vacancies, thus favoring the occupation of these sites by the Yb^{3+} ions having the ionic radius larger than that of either host ions. Hence, it seems that the n.n. Li^+ and Nb^{5+} sites are the most probable sites for formation of the dissimilar Yb^{3+}–Yb^{3+} ion pairs. It should be noticed that our model predicts that the Yb_{Li}–Yb_{Nb} pairs lie on the axis that is not parallel to the optical c (Z) axis. This is unlike the prediction of Montoya et al. [23] suggesting that the Yb_{Li}–Yb_{Nb} pairs lie along the optical c (Z) axis. Besides, the observed spectra show very low C_1 symmetry, as evidenced by the angular dependence

Author's personal copy

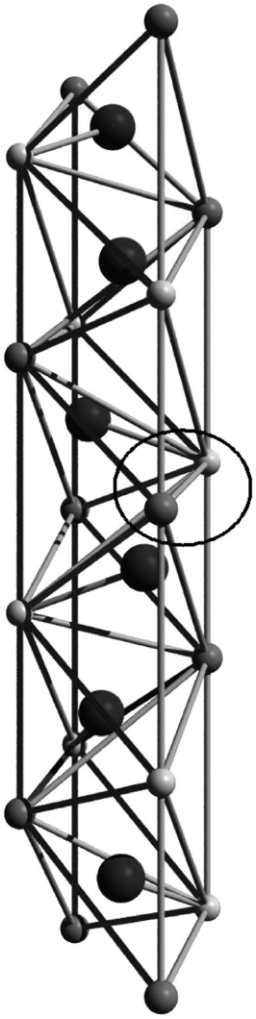

Fig. 12. Schematic structure of the nearest neighbor (n.n.) ions around Yb^{3+} ions in the LN unit cell: Li^{+} (light gray), Nb^{5+} (dark gray), and O^{2-} (black); the most probable position taken by the Yb_{Li}–Yb_{Nb} ion pair is marked by a circle.

of EPR lines (see, Figs. 3 and 4). Thus our EPR results do not support the model with the axis of the Yb_{Li}–Yb_{Nb} pair along the optical *c*-axis.

The interpretation of the experimental EPR data and thus numerical results describing the Yb_{Li}–Yb_{Nb} pairs and their locations in LN lattice are based on the simple model of the magnetic dipole–dipole interactions (Eq. (3)). In order to confirm, or disprove the present findings, further calculations using more elaborate Hamiltonians and models would be required. In this regard the feasibility of the antiferromagnetic superexchange interactions between two Yb^{3+} ions via O^{2-} ligands should receive special attention [38].

The fact that the Yb^{3+} ions in LN crystal take the positions of Li^{+} ions is not under dispute. However, what requires explanation is the mechanism which is responsible for forcing certain proportion of the Yb^{3+} ions to take the nearby Nb^{5+} positions. At present no firm description of such mechanism can be provided and various options may be considered. It appears that the presence of some co-dopant ions plays an important role in this mechanism. In Montoya et al.'s [23] study the LN crystal was co-doped by MgO. The inverse EPR line intensity (Fig. 11) shows a linear behavior in the temperature range from 40 to 70 K, whereas at higher temperatures the EPR line intensity decreases to zero as the line vanishes. This indicates that the lines observed in this temperature range do not originate from RE ions. As discussed above, an additional impurity yielding the EPR signal is observed in our LN:Yb^{3+} single crystal. Such paramagnetic impurity may unintentionally enter the LN structure from the chemical ingredients used for sample fabrication. Such contamination is highly likely in the present case due to the quality of ingredients used. The presence of unintentional impurities may act in a similar way as the co-doping by MgO [23], i.e. forcing a certain proportion of the Yb^{3+} ions to take the Nb^{5+} positions. Those Yb_{Nb} ions located nearby the Yb_{Li} sites form the $^{even}Yb^{3+}$–$^{even}Yb^{3+}$ pairs, which are apparently observed in our optical spectra and more evidently in the EPR spectra. The proposed model appears to explain well the formation of such Yb_{Li}–Yb_{Nb} pairs. Further studies are in progress in order to unravel the nature of the unintentional impurities and their effect on the magnetic and spectroscopic properties of LN:Yb^{3+} single crystals. It is worth noting that we have also carried out analysis of the EPR spectra assuming the existence of the pairs of the type $^{odd}Yb^{3+}$–$^{odd}Yb^{3+}$ or $^{odd}Yb^{3+}$–$^{even}Yb^{3+}$ ions. However, no evidence for the existence of such pairs could be identified in our EPR spectra. A possible reason may be too low resolution of our EPR X-band spectrometer. However, we did observe some additional lines in our EPR spectra that could be convincingly related rather to the isolated Yb^{3+} ions [24,25] than to the Yb^{3+}–Yb^{3+} ion pairs. Further work is now in progress to explain the origin of these lines.

4.3. Role of inequivalent single ion Yb^{3+}centers

Finally, we examine the possible explanation of the observed behavior of the temperature dependence of the EPR line as due to the presence of several different inequivalent paramagnetic centers originating from isolated Yb^{3+} ions. Let us analyze the neighborhood of the Yb^{3+} ion, assuming that Yb^{3+} ion is located at the Li^{+} site (Yb_{Li}). Fig. 13 shows the arrangement of ions in the vicinity of Yb^{3+} ion viewed along *z*-axis (optical *c*-axis, Fig. 13a) and *y*-axis (Fig. 13b) in the LN:Yb crystal. The oxygen octahedra around the impurity ions are also marked.

Replacing the Li^{+} ion by Yb^{3+} impurity requires charge compensation, which may be achieved due to vacancies occurring in the vicinity of the impurity ion. The local site symmetry of paramagnetic Yb^{3+} centers may be either C_1 or C_3 (axial) [20,21]. We focus on the crystallographically inequivalent C_1 sites since we have observed new low symmetry C_1 centers [24,25] in LN:Yb single crystal. The possible vacancies in the first shell around Yb^{3+} ion are

Author's personal copy

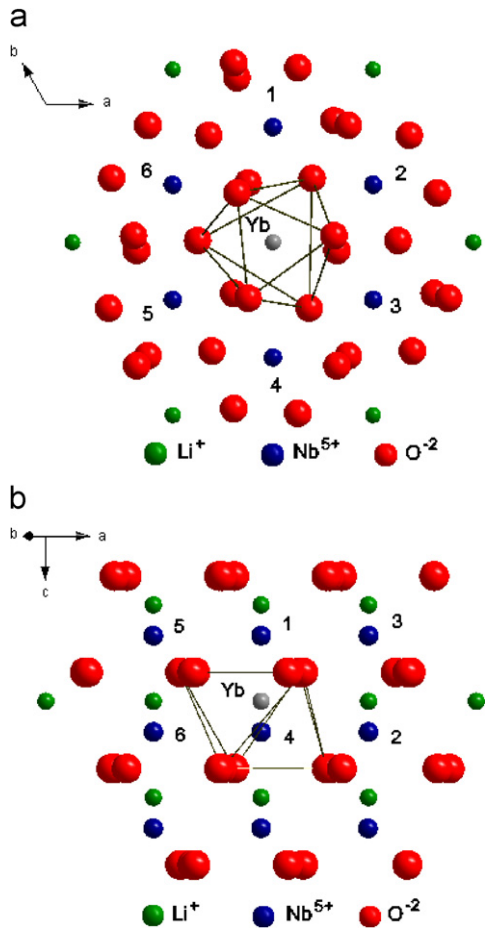

Fig. 13. Arrangement of ions in the vicinity of Yb^{3+} ions viewed along (a) z-axis (optical c-axis) and (b) y-axis in the LN: Yb crystal. Yb^{3+} ions (light gray ball in the center)—substituted at Li^{+} sites: 1, 3, 5 and 2, 4, 6-Nb^{5+} sites in the first shell "below" and "above" the Yb^{3+} ion.

indicated in Figs. 13a and b. It appears that in some papers, see, e.g. Refs. [39,40], it is assumed that in the first shell around impurity ions in doped LN single crystals three Nb^{5+} ions (1, 3, 5) and three Li^{+} ions (2, 4, 6) are present. However, it seems not to be necessarily true. The distance between Yb^{3+} and Nb^{5+} ions is equal to 0.3062 nm and 0.3363 nm for the ions 2, 4, 6 and 1, 3, 5, respectively (see Fig. 13b). The distance to Li^{+} sites, above or below the plane with Yb^{3+} ion, is equal to 0.3765 nm (see Fig. 13b). In fact, there are six Nb^{5+} sites in the first shell and six Li^{+} sites in the second shell in the plane containing Yb^{3+} ion, as depicted in Fig. 13a. Each Nb^{5+} ion at position 1–6 is connected to Yb_{Li} ion by O^{2-} bridge, so vacancies in the first shell cause tilting of the Yb^{3+} g-tensor and lowering of the local site symmetry of Yb^{3+} ions. Thus we identify six inequivalent Yb_{Li}–V_i paramagnetic centers (Yb_{Li} connected with one of V_i vacancies, $i = 1$–6), that exhibit low C_1 symmetry. It is expected that these centers dominate the EPR spectrum. All Yb_{Li}–V_i centers have the same surroundings, so the EPR lines shapes should exhibit the same thermal behavior, i.e. the temperature dependence of the intensity of EPR lines originating from these centers should behave in a similar way. It turns out that the temperature behavior of the EPR line intensity in LN:Yb single crystal cannot be related to the existence of several crystallographically inequivalent sites of single Yb^{3+} ions. Additionally, if any Yb^{3+} ion is placed at Li site and the second one is substituted for Nb^{5+} site at position 4 (see Fig. 13b), we can obtain an analogous situation as presented in Fig. 12. Note that in Fig. 12 the LN structure is not viewed along y-axis! This agreement with previous result provides an additional confirmation of the validity of our considerations.

4.4. Survey of literature indications of the presence of ion pairs in LN crystals

Our literature search has revealed several optical absorption and EPR studies dealing with formation of TM and RE ion pairs in doped lithium niobate crystals. Siu and Zhao [41] have reported that the characteristic resonance lines in the EPR spectra of LN:Cr (0.8 wt%) single crystal may be interpreted as originating from the Cr–Cr ion pairs. On the basis of the optical transmission studies on the Mg, Cr co-doped LN (7 mol% Mg and 0.5 mol% Cr) crystal, Choubey et al. [42] reported absorption bands that were attributed to the OH^{-} stretching vibration in the Mg_{Li}^{2+}–OH^{-}–Mg_{Nb}^{2+} complex. Similar phenomenon was previously observed by Kovacs et al. [43] in LN doped with Mg and co-doped with trivalent element M (M = Cr, Fe, Nd, In, Lu, Sc), who reported on the OH^{-} absorption band which they attributed to Mg_{Li}^{2+}–OH_{O}^{-} (O site)–M_{Nb}^{3+} complex. Zhao and Siu [44] have reported EPR study of the Ni^{3+}–Ni^{3+} pairs transitions in LN:Ni (0.8 wt%) single crystal, where EPR transitions were interpreted as originating from both the Ni^{3+} single ions transition as well as the Ni^{3+}–Ni^{3+} ion pairs. Additionally, Bodziony and Kaczmarek [40] have recently reported the evidence of Er_{Li}–Er_{Nb} pair formation in LN weakly doped with 0.1 wt% of Er.

5. Summary and conclusions

Optical and EPR spectroscopy measurements of LN single crystal weakly doped with Yb^{3+} ions (1 wt%) have been carried out. Analysis of the optical spectra reveals, apart from the lines originating from the isolated Yb^{3+} ions observed before, appearance of an additional bands. This observation may be considered as an indirect evidence of local perturbations arising around Yb ions.

Analysis of the temperature dependence of the EPR linewidth confirms the presence of at least two distinct paramagnetic centers in the sample. However, our results do not preclude the existence of magnetically inequivalent paramagnetic centers of the same or different type, i.e. originating from the isolated Yb^{3+} ions, or the pairs of Yb^{3+} ions. The temperature behavior of the EPR line intensity and its inverse indicates that at 8 K the spectra start showing the appearance of signals that can be

Author's personal copy

ascribed to the antiferromagnetically coupled Yb^{3+} ion pairs in LN crystal. The combined indications from the optical and EPR spectroscopy measurements provide evidence suggesting with high probability the existence of the Yb^{3+}–Yb^{3+} ion pairs in our weakly doped LN:Yb^{3+} single crystal. Deeper analysis of EPR spectra enables assignment of the observed spectral features either to the isolated Yb^{3+} ions, identified by EPR technique previously [24], or the pairs of dissimilar ions, i.e. exhibiting different g_{ij} values, of the type $^{even}Yb^{3+}$–$^{even}Yb^{3+}$ [25]. The proposed model of Yb ion pairs explains well also some unusual features observed in EPR spectra, which are related to low C_1 site symmetry. The EPR line intensity obeys the Curie–Weiss law and yields the antiferromagnetic interaction constant $\Theta = -0.6 \pm 0.3$ K. The deconvolution of the two selected EPR lines shows that EPR signals arise both from the isolated Yb^{3+} ions and the Yb^{3+}–Yb^{3+} ion pairs; the latter signals dominate.

Spectroscopic and crystallographic data suggest that most probably the $^{even}Yb^{3+}$–$^{even}Yb^{3+}$ pairs are located at the neighboring Li^+ and Nb^{5+} positions. Calculations based on the magnetic dipole–dipole interaction model indicate that the substitution of Yb^{3+} ions into LN induces an increase of about 0.1 nm in the distance, i.e. from 0.31–0.41 nm or about 34%, between the two Yb^{3+} ions forming a pair as compared with the Li^+–Nb^{5+} distance in the undistorted host [25]. The alternative explanations are also considered. The crystallographic analysis excludes the possibility that the temperature behavior of the EPR line intensity could be related to the existence of several inequivalent crystallographic sites of isolated Yb^{3+} ions in LN:Yb single crystal.

We put forward a premise that the unusual behavior of Yb^{3+} ions in weakly doped LN:Yb, i.e. formation of the Yb_{Li}–Yb_{Nb} pairs, may be facilitated by incorporation of additional, yet unidentified impurities into the crystal lattice. The qualitative framework proposed in this paper is expected to be more firmly confirmed by further studies of the nature of the mechanisms leading to formation of the $^{even}Yb^{3+}$–$^{even}Yb^{3+}$ pairs based on more elaborate models. The feasibility of the antiferromagnetic super-exchange interactions between two Yb^{3+} ions via O^{2-} ligands may be considered as an important alternative. Our results suggest that EPR signals may also be interpreted as originating from coupled paramagnetic centers, even in the case of weakly doped single crystals.

Acknowledgments

Prof. Taiju Tsuboi from Kyoto Sangyo University, Japan is deeply acknowledged for low temperature absorption measurements. This work was partially supported by the research grant from the Polish Ministry of Science and Tertiary Education in the years 2006–2009 (TB) and SMK acknowledge gratefully a DSc (habilitation) grant and a Professorial grant, respectively, from the SUT.

References

[1] J.M. Cabrera, J. Olivares, M. Carrascosa, J. Ramis, R. Muller, E. Dieguez, Adv. Phys. 45 (1996) 349.
[2] H.E. Conzett, S.I. Stepanov, Rep. Progr. Phys. 57 (1994) 39.
[3] R.S. Weis, T.K. Gaylord, Appl. Phys. A 37 (1985) 191.
[4] Properties of Lithium Niobate, EMIS Datareviews Series No. 5, Inspec 1989.
[5] S.C. Abrahams, J.M. Reddy, J.L. Bernstein, J. Phys. Chem. Solids 27 (1966) 997.
[6] S.C. Abrahams, W.C. Hamilton, J.M. Reddy, J. Phys. Chem. Solids 27 (1966) 1013.
[7] A. Lorenzo, H. Jaffrezic, B. Roux, G. Boulon, J. Garcia-Sole, Appl. Phys. Lett. 67 (25) (1995) 3735.
[8] L. Rebouta, P.J.M. Smulders, D.O. Boerma, F. Aguillo-Lopez, M.F. Da Silva, J.C. Soares, Phys. Rev. B 48 (1993) 3600.
[9] S.-Y. Wu, W.-C. Zheng, Phys. Rev. B 65 (2002) 224107.
[10] G. Burns, D.F. O'Kane, R.S. Title, Phys. Rev. B. 167 (1968) 314.
[11] C. Bonardi, C.J. Magon, E.A. Vidoto, M.C. Terrile, L.E. Bausa, E. Montoya, D. Bravo, A. Martin, F.J. Lopez, J. Alloys Compounds 323–324 (2001) 340.
[12] A. Ridah, P. Bourson, M.D. Fontana, G. Malovichko, J. Phys.: Condens. Matter 9 (1997) 55.
[13] R. Mouras, M.D. Fontana, P. Bourson, A.V. Postnikov, J. Phys.: Condens. Matter 12 (2000) 5053.
[14] R. Mouras, P. Bourson, M.D. Fontana, G. Boulon, Opt. Commun. 197 (2001) 439.
[15] M.N. Palatnikov, I.V. Biryukova, N.V. Sidorov, A.V. Denisov, V.T. Kalinnikov, P.G.R. Smith, V.Y. Shur, J. Cryst. Growth 291 (2006) 390.
[16] K. Chen, M.S. Zhang, W.C. Chen, Q. Chen, Progress in Crystal Growth and Characterization of Materials, Pergamon, Oxford, 2000, p. 41.
[17] H.-N. Dong, S.-Y. Wu, W.-C. Zheng, J. Phys. Chem. Solids 64 (2003) 695.
[18] S.H. Choh, J.H. Kim, I.W. Park, H.J. Kim, D. Choi, S.S. Kim, Appl. Magn. Reson. 24 (2003) 313.
[19] D. Bravo, A. Martin, F.J. Lopez, Solid State Commun. 112 (1999) 541.
[20] G. Malovichko, V. Grachev, E. Kokanyan, O. Shirmer, Phys. Rev. B 59 (1999) 9113.
[21] G. Malovichko, V. Grachev, Phys. Rev. B 62 (2000) 7779.
[22] E. Montoya, O. Espeso, L.E. Bausa, J. Lumin. 87–89 (2000) 1036.
[23] E. Montoya, L.E. Bausa, B. Schaudel, P. Goldner, J. Chem. Phys. 114 (2001) 3200.
[24] T. Bodziony, S.M. Kaczmarek, Opt. Mater. 29 (2007) 1440.
[25] T. Bodziony, S.M. Kaczmarek, Res. Chem. Intermed., RCI 33/8-9, 2007, available online.
[26] T. Bodziony, S.M. Kaczmarek, J. Hanuza, J. Alloys Compounds, 2007, doi:10.1016/j.jallcom.2007.04.189.
[27] I. Pracka, M. Malinowski, A.L. Bajor, B. Surma, Z. Gałązka, M. Świrkowicz, M. Możdżonek, Proc. SPIE 3178 (1997) 295.
[28] T. Tsuboi, S.M. Kaczmarek, G. Boulon, J. Alloys Compounds 380 (2004) 196.
[29] A. Lorenzo, H. Loro, J.E. Munoz Santistute, M.C. Terrile, G. Boulon, J. Garcia Sole, Opt. Mat. 8 (1997) 55.
[30] E. Montoya, J.A. Sanz-Garcia, L.E. Bausa, Spectrochim. Acta A 54 (1998) 2081.
[31] E. Montoya, A. Lorenzo, L.E. Bausa, J. Phys.: Condens. Matter 11 (1999) 311.
[32] P.H. Haumesser, R. Gaume, B. Viana, E. Antic-Fidancev, D. Vivien, J. Phys.: Condens. Matter 13 (2001) 5427.
[33] S. Campos, A. Denoyer, S. Jandl, B. Viana, D. Vivien, P. Loiseau, B. Ferrand, J. Phys.: Condens. Matter 16 (2004) 4579.
[34] A.V. Postnikov, V. Caciuc, G. Borstel, J. Phys. Chem. Solids 61 (2000) 295.

Author's personal copy

[35] A. Abragam, B. Bleaney, Electron Paramagnetic Resonance of Transition Ions, Clarendon Press, Oxford, 1970.
[36] J.R. Pilbrow, Transition Ion Electron Paramagnetic Resonance, Clarendon Press, Oxford, 1990.
[37] O. Guillot-Noel, P. Goldner, P. Higel, D. Gournier, J. Phys.: Condens. Matter 16 (2004) R1.
[38] A. Bencini, D. Gatteschi, Electron Paramagnetic Resonance of Exchange Coupled Systems, Springer, Berlin, 1990.
[39] D. Xue, X. He, Phys. Rev. B 73 (2006) 064113.
[40] T. Bodziony, S.M. Kaczmarek, Physica B (2007), doi:10.1016/j.physb.2007.06.032.
[41] G.G. Siu, M.-G. Zhao, Phys. Rev. B. 43 (1991) 13575.
[42] R.K. Choubey, P. Sen, S. Kar, G. Bhagavannarayana, K.S. Bartwal, Solid State Commun. 140 (2006) 120.
[43] L. Kovacs, L. Rebouta, J.C. Soares, M.F. da Silva, A.M. Hage, J.P. Stoquert, P. Siffetr, G.J.A. Sanz, G. Corradi, Z.s. Szaller, K. Polgar, J. Phys.: Condens. Matter 5 (1993) 781.
[44] M.-G. Zhao, G.G. Siu, Phys. Rev. B. 51 (1995) 6246.